textiles

MDPI

Article

Circular Valorization of Post-Industrial Textile Waste in Thermal-Insulating Cementitious Ceiling Sheets

Kavini Vindya Fernando [1], Charith Akalanka Dodangodage [2,*], Vinalee Maleeshi Seneviratne [1], Sanduni Maleesha Jayasinghe [1], Dhammika Dharmaratne [3], Geethaka Nethsara Gamage [2], Ranoda Hasandee Halwatura [2], U. S. W. Gunasekera [1] and Rangika Umesh Halwatura [2]

[1] Department of Textile and Apparel Engineering, University of Moratuwa, Moratuwa 10400, Sri Lanka; kavinivindya2000@gmail.com (K.V.F.)
[2] ProGreen Laboratory, Department of Civil Engineering, University of Moratuwa, Moratuwa 10400, Sri Lanka; rangika@uom.lk (R.U.H.)
[3] Department of Civil Engineering, Sri Lanka Institute of Information Technology, New Kandy Road, Malabe 10115, Sri Lanka; dhammika.dh@sliit.lk
* Correspondence: dodangodageca.24@uom.lk

Abstract

The construction sector faces increasing pressure to reduce the embodied energy of building materials while valorizing industrial waste streams. This study evaluates the direct incorporation of post-industrial textile waste (100% cotton and cotton–polyester blends) in its native form to develop high-performance cementitious ceiling sheets. Composites were fabricated under a controlled hydraulic compaction pressure of 2.0 MPa, optimized to achieve matrix densification while preserving the integrity of the fibrous network. Viscoelastic recovery of the compressed fibers induced a hierarchical double-porosity architecture characterized by macro-voids and hollow fiber lumens. This microstructural evolution reduced thermal conductivity to 0.091 W/m·K, approximately 50% lower than commercial cement–fiber benchmarks—without compromising mechanical compliance. Scanning Electron Microscopy (SEM) revealed a mechanistic decoupling between water absorption and dimensional stability. Although the CP15 formulation (15 wt.% cotton–polyester) exhibited high moisture uptake (~21%), thickness swelling remained limited to 1.35%. This dimensional stability is attributed to the hydrophobic polyester framework, which bridges microcracks and constrains hygroscopic expansion within the cellulosic phase. The optimized CP15 composite achieved a Modulus of Rupture (MOR) of 8.75 MPa, exceeding ISO 8336 Category C, Class 2 requirements. Despite increased thickness, the areal density (10.84 kg/m^2) remains compatible with standard gypsum-grade suspension systems, eliminating the need for structural modification. These findings establish a scalable, direct-valorization strategy for circular construction materials delivering enhanced thermal insulation and robust performance under tropical climatic conditions.

Keywords: textile waste valorization; cementitious ceiling sheets; thermal conductivity; dimensional stability; circular economy; sustainable construction

Academic Editor: Rajesh Mishra

Received: 31 December 2025
Revised: 16 February 2026
Accepted: 17 February 2026
Published: 27 February 2026

1. Introduction

Rapid population growth, accelerated urbanization, and rising living standards have substantially increased global demand for construction materials, energy, and infrastructure. These trends have driven a sustained rise in carbon dioxide (CO_2) emissions and solid waste generation, placing unprecedented pressure on natural ecosystems and the built

environment [1–3]. Among emerging environmental challenges, the textile and apparel industry has become a major contributor, generating approximately 92 million tonnes of textile waste annually, a figure projected to reach 134 million tonnes by 2030 in the absence of effective mitigation strategies [4]. The sector accounts for nearly 10% of global greenhouse gas emissions and approximately 20% of industrial wastewater generation worldwide [5]. In Europe alone, textile consumption results in an estimated 654 kg of CO_2-equivalent emissions per capita per year [6]. Despite containing valuable fibrous resources, the majority of textile waste is disposed of through landfilling or incineration, contributing to land degradation and, in the case of synthetic textiles, persistent microplastic pollution [7,8].

These global pressures are strongly reflected in developing economies such as Sri Lanka, where the textile and apparel industry represents a major economic pillar while simultaneously generating substantial quantities of fabric and yarn waste during manufacturing processes [9]. In the absence of dedicated textile recycling infrastructure, this waste is predominantly managed through export, co-processing in cement kilns, or direct landfilling [9,10]. Although such approaches enable partial diversion, they do not achieve long-term material circularity or high-value resource recovery. Recent advances in sustainable engineering emphasize that circularity must extend across diverse waste streams, including the bioremediation of liquid effluents [11,12], integrated nutrient recovery systems [13,14], and the upcycling of solid industrial by-products. Accordingly, the valorization of textile waste into cementitious construction materials has gained increasing attention as a strategy to reduce environmental burdens while preserving functional performance, consistent with circular economy principles [15–18].

Within the construction sector, cement fiber ceiling sheets represent a high-volume yet comparatively underexplored application for textile waste integration. Unlike structural elements, ceiling panels prioritize low bulk density for safe overhead installation, thermal resistivity for indoor comfort, and dimensional stability under fluctuating humidity rather than high compressive strength [19]. Commercial cement fiber ceiling sheets remain widely used in low-income regions of Latin America, Africa, and South Asia due to their affordability, ease of installation, and durability under harsh climatic conditions [18]. However, conventional products typically exhibit bulk densities of approximately 1350–1450 kg/m^3 and thermal conductivity values ranging from 0.15 to 0.19 W/m·K, which contribute to conductive heat transfer and reduced indoor thermal comfort. These limitations highlight the need for thermally enhanced cementitious ceiling sheets capable of achieving thermal conductivity values below 0.15 W/m·K while maintaining adequate flexural performance for non-structural applications [20–22].

Post-industrial textile fabric waste presents a promising fibrous reinforcement for addressing these performance gaps; however, composite behavior is strongly governed by fiber composition and fiber–matrix interfacial interactions. Cotton fibers, being hydrophilic and cellulose-rich, generally exhibit favorable bonding with cement hydration products but are prone to moisture uptake and dimensional instability [23–25]. In contrast, polyester fibers are hydrophobic and offer improved durability and moisture resistance, yet often demonstrate limited interfacial adhesion due to their smooth surface morphology. Blended textile waste therefore offers the potential to harness synergistic benefits: enhanced bonding from the hydrophilic cotton fraction and improved dimensional stability from the hydrophobic polyester fraction. Despite the global abundance of cotton- and polyester-based waste streams, optimization of their combined use—particularly in blended textile formats for thin cementitious ceiling sheets—remains insufficiently explored [26–28].

Conventional textile waste valorization strategies typically involve energy-intensive chemical scouring to remove industrial sizing agents, thereby increasing the embodied

energy of the recycled product. This study challenges that paradigm by investigating a direct-valorization pathway that utilizes textile waste in its native industrial state. It is hypothesized that residual surface treatments may act as passive interfacial modifiers, while elastic recovery of the fibrous network during compaction induces a hierarchical "double-porosity" microstructure composed of macro-voids and hollow fiber lumens, thereby enhancing thermal insulation performance.

In response to these research gaps, this study evaluates the feasibility of incorporating post-industrial 100% cotton [29,30] and cotton–polyester (60/40) blended waste [31,32] as reinforcement in cementitious ceiling sheets. The primary objectives are: (1) to systematically evaluate the influence of fiber loading (5–30 wt.%) on the physical, mechanical, and thermal properties of the composites; (2) to elucidate the trade-offs among density reduction, spring-back-induced porosity, and flexural integrity; and (3) to benchmark the performance of these waste-valorized composites against commercial cement fiber ceiling sheets. By engineering a functional construction material from untreated industrial by-products, this research proposes a scalable, low-energy pathway aligned with circular economy principles.

2. Methods

2.1. Materials Characterization

2.1.1. Cementitious Binding Matrix

Ordinary Portland Cement (OPC) of strength class 42.5 N, conforming to SLS 107:2015, was employed as the hydraulic binding matrix. This cement grade was selected due to its rapid early-age strength development, consistent hydration kinetics, and demonstrated chemical compatibility with hydrophilic cellulosic fibers in fiber-reinforced cementitious composite systems [33,34]. The key physical and mechanical properties of the cement, as provided by the manufacturer, Tokyo cement, Colombo, Sri Lanka, are summarized in Table 1.

Table 1. Physical and Mechanical Properties of Ordinary Portland Cement (OPC).

Property	Value
Specific gravity (g/cm^3)	3.15
Blaine fineness (cm^2/g)	3540
Initial setting time (min)	200
Final setting time (min)	280
2-day compressive strength (MPa)	25.3
7-day compressive strength (MPa)	40.5
28-day compressive strength (MPa)	51.7

2.1.2. Reinforcing Phase

Two distinct post-industrial textile waste streams were utilized as fibrous reinforcement phases: 100% cotton woven fabric waste and a cotton–polyester blended knitted fabric.

1. 100% Cotton Waste: Sourced from a leading home textile manufacturer in Sri Lanka, this waste stream primarily consists of fabric off-cuts and defective materials generated during cutting and inspection. Cotton was selected for its inherent biodegradability, low density, and high tensile strength (typically 287–800 MPa), which serves to enhance the mechanical integrity of cementitious composites while minimizing environmental impact.

Furthermore, the hollow lumen structure of cotton fibers offers superior thermal insulation potential, making it an ideal candidate for ceiling sheet applications [29,30,35].

2. Cotton–Polyester Blend (60/40): The second waste stream, a knitted greige fabric, was obtained from a prominent export-oriented textile factory. The specific composition of 60% cotton and 40% polyester was selected as it represents a "fast-moving" production specification within the Sri Lankan apparel sector. This dominance in the local manufacturing landscape ensures a consistent, high-volume supply of waste material, which is critical for the industrial scalability of the proposed recycling pathway. Scientifically, this blend ratio offers a synergistic balance: the cotton fraction contributes to thermal resistance and cement compatibility, while the polyester fraction enhances durability and moisture resistance [31,36].

Key physical characteristics were determined in accordance with ASTM D3776 for mass per unit area (GSM) and ASTM D3775 for yarn density (fabric count) to evaluate reinforcement potential and dispersion behavior within the cementitious matrix [29–31,35]. The measured properties of the waste fabrics are summarized in Table 2.

Table 2. Characteristics of Waste Fabrics Used as Reinforcement.

Characteristic	100% Cotton	Cotton–Polyester Blend (60/40)
Fabric type	Woven	Knitted
Specific weight (g/m^2)	120.9	181.5
Yarn density (threads/inch)	PPI-60, EPI-39	CPI-56, WPI-28

To elucidate the structural differences between the reinforcement types, SEM analysis was conducted on the as-received fabrics (Figure 1). The 100% cotton reinforcement exhibits a woven architecture characterized by orthogonal yarn interlacing, resulting in a relatively open structure with a lower specific weight (120.9 g/m^2). In contrast, the cotton–polyester blend features a knitted architecture composed of interlocking loops. This looped geometry facilitates a higher packing density of fiber bundles per unit area, which explains its significantly higher specific weight (181.5 g/m^2) compared to the woven cotton fabric, despite the lower intrinsic density of polyester fibers (1.38 g/cm^3) relative to cellulose (1.54 g/cm^3). This structural densification is critical for enhancing the mechanical anchoring of the reinforcement within the cementitious matrix.

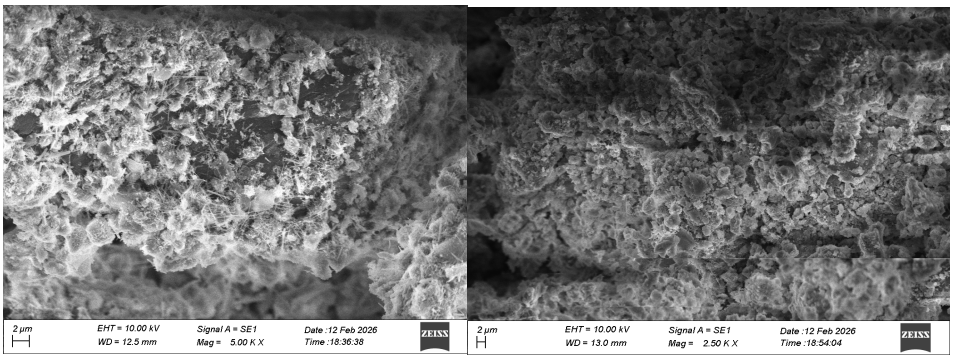

(**a**) (**b**)

Figure 1. Scanning Electron Microscopy (SEM) micrographs of the textile reinforcement in its native state: (**a**) 100% Cotton woven fabric showing orthogonal fiber interlacing; (**b**) Cotton–Polyester knitted fabric showing dense, looped yarn architecture.

2.2. Sample Preparation

2.2.1. Processing of Textile Reinforcement

To promote uniform dispersion within the cementitious matrix and minimize fiber agglomeration, the textile wastes were mechanically processed using a rotary shredding machine (Figure 2). Multiple shredding cycles were evaluated during a preliminary optimization phase to determine the fiber aspect ratio most suitable for thin cementitious sheet fabrication.

Figure 2. Mechanical processing sequence of post-industrial textile waste: (**a**) The rotary shredding machine utilized for fiber size reduction; (**b**) Raw textile waste off-cuts prior to processing; (**c**) The resulting shredded fiber mass after the second shredding cycle, illustrating the degree of fiber disentanglement and fluffing used for composite fabrication.

Fiber length distribution was characterized by collecting a random sample of fibers (n = 100) from each shredding batch. The lengths were measured using high-resolution digital imaging and analyzed via ImageJ (1.54p version) software to determine the arithmetic mean.

Based on the analysis, the second shredding cycle was selected as it yielded an optimal average fiber length of approximately 10 mm (Table 3). This length provided the most effective balance between rheological performance and reinforcement efficiency; specifically, it avoided the "balling" effect observed with longer fibers (Cycle 1) while ensuring sufficient aspect ratio for crack-bridging, which was compromised in the shorter fibers (Cycle 3).

Table 3. Average Fiber Lengths Obtained from Different Shredding Cycles.

Shredding Cycle	Average Fiber Length (mm)
1st cycle	12
2nd cycle (selected)	10
3rd cycle	7

2.2.2. Mix Design and Fabrication Protocol

All composites were fabricated using a fixed water-to-cement (w/c) ratio of 0.6 and a hydraulic pressing pressure of 2 MPa, consistent with established processing protocols for fiber–cement sheet materials [37–40].

The experimental program comprised 11 mix formulations, incorporating textile fibers at contents of 5, 10, 15, 20, and 30 wt.%, relative to the total dry composite mass, for both textile types. Each formulation targeted a total specimen mass of 250 g. The detailed mix proportions are summarized in Table 4.

Table 4. Experimental Mix Proportions and Sample Plan.

Fiber Content (wt.%)	Cement Matrix (wt.%)	Mix Code (Cotton)	Mix Code (Cotton–Poly)
0	100	CNTRL	—
5	95	C05	CP05
10	90	C10	CP10
15	85	C15	CP15
20	80	C20	CP20
30	70	C30	CP30

The fresh mixtures were cast into steel molds with dimensions of 150 × 150 × 50 mm. Compaction pressure was selected based on a preliminary optimization study where varying pressures (0.5, 1.0, 1.5, 2.0, and 2.5 MPa) were evaluated. The results indicated that a pressure of 2 MPa yielded optimal mechanical consolidation without causing excessive dewatering or fiber crushing. Consequently, all subsequent specimens were compacted using a hydraulic press at a constant pressure of 2 MPa, as illustrated in Figure 3. Specimens were cured for 28 days under ambient laboratory conditions. To ensure adequate hydration during early curing, specimen surfaces were moistened daily for the first 7 days [41].

Figure 3. Fabrication process of the ceiling sheets: (**a**) Fresh fiber–cement mixture placed in 150 × 150 mm steel molds; (**b**) Hydraulic compaction of the specimens at 2 MPa; (**c**) Demolded specimens during the initial curing phase.

2.2.3. Commercial Reference Ceiling Sheets

To assess the practical feasibility and industrial relevance of the developed composites, experimental results were benchmarked against commercial cement fiber ceiling sheets commonly used in the local construction sector. Two representative product categories were selected:

- Commercial cement fiber ceiling sheets (legacy formulation)—representing conventional high-strength market products
- Commercial cellulose fiber–reinforced cement ceiling sheets—representing widely adopted contemporary alternatives

The commercial sheets were cut to dimensions matching the experimental specimens (150 × 150 mm for physical and thermal testing and 150 × 20 mm for mechanical testing) to ensure direct and consistent comparative evaluation.

2.3. Characterization Methodologies

All physical, mechanical, and thermal characterizations were conducted on both experimental composites and commercial reference ceiling sheets under identical laboratory conditions to minimize experimental variability.

2.3.1. Physical Properties

Physical characterization was performed to evaluate the influence of fiber incorporation on matrix compaction, pore development, and bulk material properties.

Dimensional Stability (Thickness): Specimen thickness was measured at four distinct locations using a digital vernier caliper with 0.01 mm precision to assess compaction uniformity.

Apparent Density: Apparent density was determined in accordance with ISO 8336:2017 [42]. Specimens were saturated in water for 24 h to determine displaced volume (V), followed by oven drying at 100 ± 5 °C to constant mass (m). Standard calculation methods defined in the cited standard were employed.

Water Absorption: Water absorption was evaluated following ASTM C1185-08. Specimens were oven-dried at 90 ± 2 °C to obtain the dry mass (W_d) [43], then immersed in water for 48 h to obtain the saturated mass (W_s). Absorption percentages were calculated as per the protocols specified in the standard.

2.3.2. Mechanical Properties

Flexural Performance (Modulus of Rupture, MOR): Flexural strength, expressed as Modulus of Rupture (MOR), was determined using a three-point bending configuration in accordance with ISO 8336:2017 and SLS 1593:2018. Specimens of dimensions 150 × 20 mm were tested at a span length of 50 mm [42,44]. A constant displacement rate of 20 mm/min was applied until failure. Five replicates were tested for each formulation.

2.3.3. Thermal Performance

Thermal Conductivity: Thermal conductivity was measured using the steady-state Lee's Disk method, in alignment with principles outlined in ASTM C518-21 [45]. Specimens were conditioned at 22 °C, and specimen edges were insulated to minimize lateral heat losses. The system was allowed to reach thermal equilibrium using a steam chamber maintained at 80 °C

2.3.4. Microstructural Analysis

The microstructural morphology of fractured composite surfaces was examined using Scanning Electron Microscopy (SEM) to elucidate fiber dispersion, fiber–matrix interfacial

bonding behavior, Interfacial Transition Zone (ITZ) integrity, and pore distribution. Comparative analysis was performed between the reference composite (C20) and the optimized formulations (C15 and CP15/CP20), enabling evaluation of reinforcement efficiency and interfacial modification mechanisms.

Prior to imaging, specimens were oven-dried at 105 °C for 24 h to eliminate residual moisture and subsequently sputter-coated with a thin gold layer to prevent electrostatic charging. Imaging was conducted using a Zeiss EVO 18 microscope (Carl Zeiss Microscopy GmbH, Oberkochen, Germany) operating in Secondary Electron (SE) mode at an accelerating voltage of 10–15 kV.

Microstructural observations focused on:

(i) fiber pull-out and crack-bridging mechanisms;
(ii) interfacial debonding gaps and ITZ continuity;
(iii) preservation of hollow fiber lumens;
(iv) the distribution and morphology of micro-voids within the cementitious matrix.

This approach enabled correlation between processing-induced microstructural evolution and the measured mechanical and thermal performance of the composites.

2.3.5. Dimensional Stability and Moisture Movement

To assess the durability and dimensional stability of the composites under extreme moisture exposure, a total immersion test was conducted in accordance with ISO 8336 [46]. Specimens were conditioned to a constant dry mass, and their initial dimensions (length, width, and thickness) were recorded using a digital vernier caliper (0.01 mm precision). The samples were then fully immersed in water at ambient temperature (27 ± 2 °C) for 24 h. Post-immersion dimensions were recorded, and the percentage of dimensional swelling (thickness, length, and width) was calculated relative to the initial dry dimensions, as prescribed by the standard.

2.4. Statistical Analysis

All experimental tests were conducted in triplicate, and results are reported as mean ± standard deviation. Statistical significance was evaluated using one-way analysis of variance (ANOVA) at a 95% confidence level ($\alpha = 0.05$). Where statistically significant differences were detected, Tukey's post hoc test was applied for pairwise comparisons.

3. Results

3.1. Physical Properties

3.1.1. Process Optimization and Compaction Pressure

To determine the critical manufacturing parameters, a preliminary optimization study was conducted by varying the hydraulic compaction pressure from 0.5 to 2.5 MPa. The physical integrity and microstructural quality of the fresh composites were evaluated immediately after demolding.

As summarized in Table 5, a non-linear relationship was observed between pressure and consolidation efficiency. Lower pressures (<1.5 MPa) failed to achieve sufficient particle packing, resulting in composites with low green strength that crumbled during handling. Conversely, increasing the pressure to 2.5 MPa caused excessive dewatering, where the cement paste was forced out of the mold along with the filtrate water ("cement washout"), leaving a fiber-rich, binder-deficient surface. Additionally, microscopic inspection at 2.5 MPa revealed signs of fiber crushing, which compromises the thermal insulation potential of the hollow lumens.

Table 5. Optimization of hydraulic compaction pressure and observed manufacturing defects.

Compaction Pressure (MPa)	Matrix Consolidation State	Fiber Integrity	Observed Defects	Suitability
0.5	Very Poor	Intact	Friable edges; extensive delamination upon demolding.	Rejected
1.0	Poor	Intact	High porosity; insufficient green strength for handling.	Rejected
1.5	Moderate	Intact	Minor surface dusting; partial recovery of thickness.	Rejected
2.0	Optimal	Intact	Uniform surface; stable geometry; controlled dewatering.	Selected
2.5	High	Compromised	Excessive dewatering (cement washout); localized fiber crushing.	Rejected

Consequently, 2.0 MPa was identified as the optimal pressure, balancing adequate mechanical consolidation with the preservation of the fiber reinforcement's porous structure. All subsequent specimens for physical and mechanical characterization were fabricated using this optimized parameter.

3.1.2. Dimensional Stability and Thickness Swelling

The thickness variation in the cured cementitious ceiling sheets, benchmarked against six commercially available cement fiber ceiling sheet products, is presented in Figure 3. One-way analysis of variance (ANOVA) confirmed that both reinforcement type and fiber loading level exerted a statistically significant influence on final specimen thickness ($p < 0.05$).

As shown in Figure 4, the commercial cement fiber ceiling sheets of legacy formulation (CM01–CM04) exhibited the lowest thickness values, ranging from 3.53 to 4.62 mm, forming a statistically distinct group (Group a). In contrast, the commercial cellulose fiber–reinforced cement ceiling sheets (CM05 and CM06) displayed significantly higher thickness values between 5.50 and 6.00 mm and were classified within Group b.

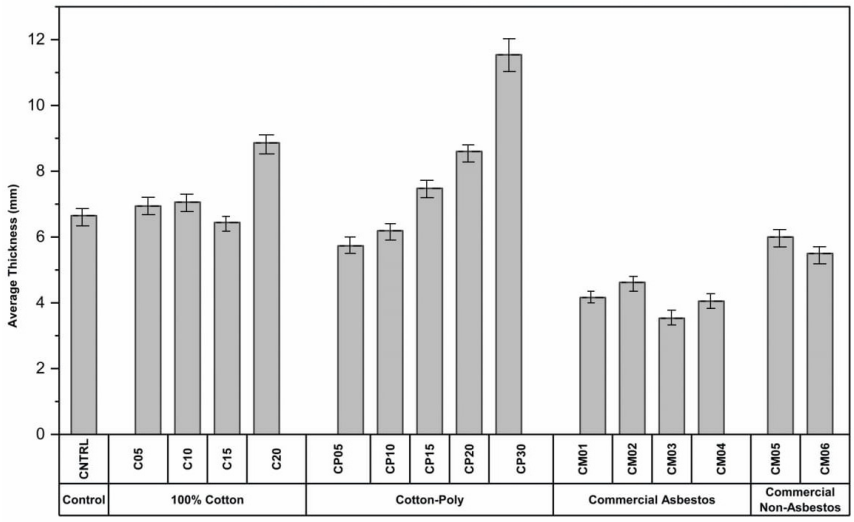

Figure 4. Comparative thickness development of textile-reinforced cementitious ceiling sheets relative to commercial cement fiber ceiling sheets.

Tukey's post hoc comparison revealed no statistically significant difference ($p > 0.05$) between the cellulose fiber–cement ceiling sheets and the cotton–polyester reinforced

composites at lower fiber loadings. In particular, CP05 (5.73 ± 0.19 mm) and CP10 (6.19 ± 0.39 mm) were grouped together with the commercial cellulose fiber–cement products, indicating comparable dimensional development under identical pressing conditions.

With increasing fiber incorporation, a progressive increase in specimen thickness was observed across both reinforcement systems. This behavior is attributed to the elastic recovery ("spring-back") of the textile fibers following the release of hydraulic pressure, a phenomenon that prevents complete matrix densification and generates residual microvoids. The CP30 formulation exhibited the highest thickness value (11.54 ± 0.35 mm), forming a statistically distinct group (Group e). Intermediate fiber contents (15–20 wt.%) resulted in moderate thickness increases, with values distributed across Groups c and d.

The complete statistical grouping of thickness values for all experimental and commercial ceiling sheet specimens is summarized in Table 6.

Table 6. Thickness development with Tukey's statistical grouping.

Sample Code	Reinforcement Type	Average Thickness (mm)
C05	100% Cotton (5%)	6.94 ± 0.59 ^{c}
C10	100% Cotton (10%)	7.06 ± 0.98 ^{c}
C15	100% Cotton (15%)	6.44 ± 0.47 ^{b}
C20	100% Cotton (20%)	8.86 ± 0.27 ^{d}
CP05	Cotton–Poly (5%)	5.73 ± 0.19 ^{b}
CP10	Cotton–Poly (10%)	6.19 ± 0.39 ^{b}
CP15	Cotton–Poly (15%)	6.65 ± 0.31 ^{c}
CP20	Cotton–Poly (20%)	7.48 ± 0.62 ^{c}
CP30	Cotton–Poly (30%)	11.54 ± 0.35 ^{e}
CM01	Commercial Asbestos	4.16 ± 0.23 ^{a}
CM02	Commercial Asbestos	4.62 ± 0.20 ^{a}
CM03	Commercial Asbestos	3.53 ± 0.23 ^{a}
CM04	Commercial Asbestos	4.05 ± 0.20 ^{a}
CM05	Commercial Non-Asbestos	6.00 ± 0.25 ^{b}
CM06	Commercial Non-Asbestos	5.50 ± 0.20 ^{b}

Note: Values represent mean ± standard deviation. Means sharing the same superscript letter are not statistically different according to Tukey's post hoc test ($p > 0.05$).

Although identical mold dimensions and a constant hydraulic pressing pressure were applied to all formulations, noticeable variations in final specimen thickness were observed with increasing textile fiber content. This behavior is attributed to the viscoelastic recovery ('spring-back') of the textile reinforcement following the release of hydraulic pressure. In this study, a standardized short pressure duration was employed to maintain experimental consistency; however, this allowed for partial elastic recovery of the fibrous network, hindering maximal matrix densification.

It is important to note that this is a processing characteristic rather than an inherent material defect. In large-scale industrial manufacturing, this dimensional variation can be effectively mitigated by optimizing the pressure dwell time to allow for complete stress relaxation within the fiber reinforcement or by calibrating the mold geometry to account for the specific compressibility factor of the textile waste. Therefore, the reduced densities observed in this study represent a conservative baseline that can be further enhanced through process engineering.

3.1.3. Apparent Density

The apparent density of the textile-reinforced cementitious ceiling sheets, benchmarked against commercial cement fiber ceiling sheets, is presented in Figure 5, with statistical groupings summarized in Table 7. ANOVA confirmed that fiber loading had a statistically significant effect on apparent density ($p < 0.05$).

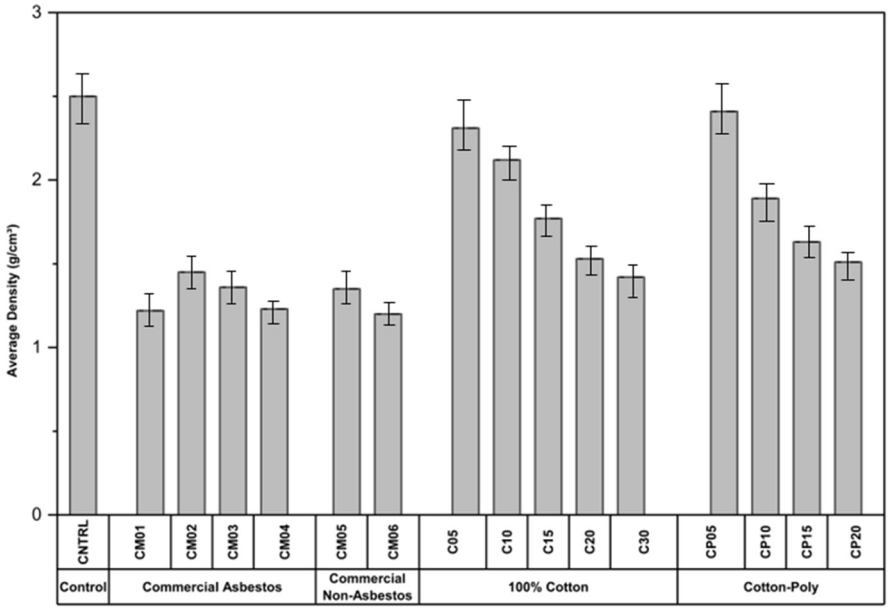

Figure 5. Influence of textile fiber content on apparent density relative to commercial cement fiber ceiling sheets.

Table 7. Apparent Density with Tukey's Statistical Grouping.

Sample Code	Reinforcement Type	Average Density (g/cm^3)
CNTRL	Control (Cement Only)	2.50 ± 0.13 ^{a}
C05	100% Cotton (5%)	2.31 ± 0.12 ^{b}
C10	100% Cotton (10%)	2.12 ± 0.09 ^{c}
C15	100% Cotton (15%)	1.77 ± 0.10 ^{d}
C20	100% Cotton (20%)	1.53 ± 0.07 ^{e}
C30	100% Cotton (30%)	1.42 ± 0.06 ^{f}
CP05	Cotton–Poly (5%)	2.41 ± 0.11 ^{b}
CP10	Cotton–Poly (10%)	1.89 ± 0.14 ^{d}
CP15	Cotton–Poly (15%)	1.63 ± 0.08 ^{e}
CP20	Cotton–Poly (20%)	1.51 ± 0.09 ^{e}
CP30	Cotton–Poly (30%)	1.48 ± 0.11 ^{e}
CM01	Commercial Asbestos	1.22 ± 0.06 ^{f}
CM02	Commercial Asbestos	1.45 ± 0.07 ^{f}
CM03	Commercial Asbestos	1.36 ± 0.06 ^{f}
CM04	Commercial Asbestos	1.23 ± 0.05 ^{f}
CM05	Commercial Non-Asbestos	1.35 ± 0.07 ^{f}
CM06	Commercial Non-Asbestos	1.20 ± 0.05 ^{g}

Note: Values represent mean ± standard deviation. Means sharing the same letter are not statistically different according to Tukey's post hoc test ($p > 0.05$).

Relative to the control (2.50 ± 0.13 g/cm^3), the incorporation of textile fibers induced a pronounced, non-linear reduction in apparent density. At low fiber loadings (5 wt.%), the density reduction was marginal (4–8%), indicating that the cement matrix remained the dominant phase. However, a precipitous drop was observed as fiber content increased beyond 10 wt.%, marking a transition zone where the low-density fibrous network began to govern the composite's bulk volume.

This trend effectively plateaued beyond 20 wt.%, suggesting a maximum packing limit for the fibers. Ultimately, at 30 wt.% loading, the apparent density was reduced by approximately 43.2% (to 1.42 g/cm^3) for cotton and 40.8% (to 1.48 g/cm^3) for cotton–polyester composites. This significant lightening confirms that the 'spring-back' effect described in Section 3.1.1 exerts a disproportionate influence at higher volume fractions, effectively diluting the heavy cementitious matrix.

As illustrated in Figure 5, comparisons with commercial benchmarks reveal that experimental composites containing 15–30 wt.% textile fibers achieved density values statistically comparable ($p > 0.05$) to market products. Notably, while the control density was excessive, the optimized formulations CP15 (1.63 ± 0.08 g/cm^3) and CP20 (1.51 ± 0.09 g/cm^3) achieved density reductions of 35% and 40% respectively, aligning them directly with the commercial cement fiber ceiling sheets (Groups f and g) required for lightweight ceiling applications.

3.1.4. Water Absorption Behavior

The water absorption behavior of the experimental composites and commercial cement fiber ceiling sheets is presented in Figure 6, with statistical groupings summarized in Table 8. ANOVA confirmed that both reinforcement type and fiber loading had a statistically significant effect on water absorption capacity ($p < 0.05$).

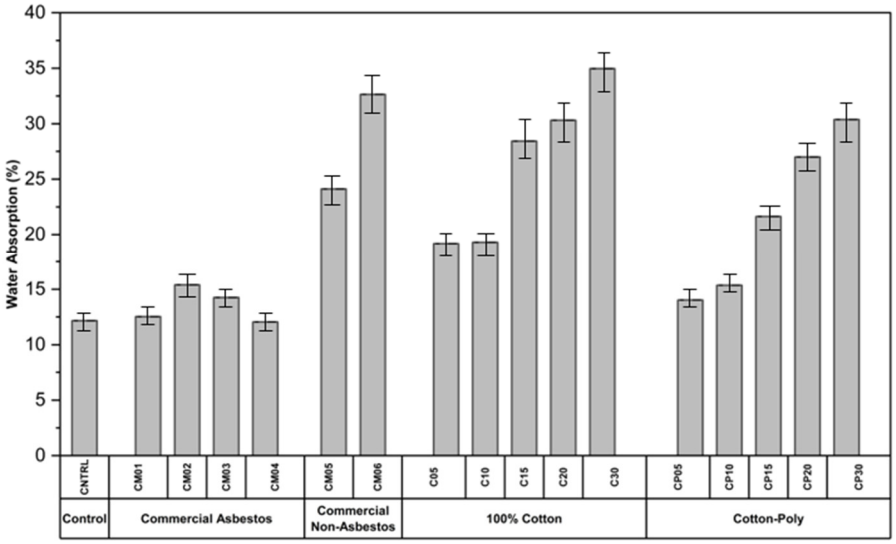

Figure 6. Water absorption behavior of textile-reinforced cementitious ceiling sheets compared with commercial products.

The cement-only control specimens exhibited the lowest water absorption (12.17 ± 0.48%), forming a statistically distinct group (Group a). The commercial cement fiber ceiling sheets of legacy formulation (CM01–CM04) displayed similarly low water absorption values (12.04–15.39%), reflecting relatively dense microstructures and limited open pore connectivity.

Table 8. Water Absorption Analysis with Statistical Grouping. Values represent Mean ± Standard Deviation (SD). Means sharing the same superscript letter are not statistically different ($p > 0.05$).

Sample Code	Reinforcement Type	Water Absorption (Mass %)
CNTRL	Control (Cement Only)	12.17 ± 0.48^{a}
C05	100% Cotton (5%)	19.18 ± 0.85^{c}
C10	100% Cotton (10%)	19.31 ± 0.79^{c}
C15	100% Cotton (15%)	28.43 ± 1.25^{f}
C20	100% Cotton (20%)	30.31 ± 1.35^{g}
C30	100% Cotton (30%)	34.96 ± 1.55^{h}
CP05	Cotton–Poly (5%)	14.02 ± 0.61^{ab}
CP10	Cotton–Poly (10%)	15.36 ± 0.68^{b}
CP15	Cotton–Poly (15%)	21.64 ± 0.95^{d}
CP20	Cotton–Poly (20%)	27.01 ± 1.15^{f}
CP30	Cotton–Poly (30%)	30.38 ± 1.28^{g}
CM01	Commercial Asbestos	12.53 ± 0.30^{a}
CM02	Commercial Asbestos	15.39 ± 0.65^{b}
CM03	Commercial Asbestos	14.25 ± 0.52^{ab}
CM04	Commercial Asbestos	12.04 ± 0.44^{a}
CM05	Commercial Non-Asbestos	24.12 ± 1.06^{e}
CM06	Commercial Non-Asbestos	32.64 ± 1.45^{gh}

For the textile-reinforced composites, water absorption increased progressively with fiber loading for both reinforcement systems, consistent with increased capillary pore volume and fiber-induced pore connectivity. The cotton-reinforced series exhibited systematically higher absorption values than the cotton–polyester composites, attributable to the hydrophilic and cellulose-rich nature of cotton fibers. Water absorption increased from 19.18 ± 0.85% (C05) to 34.96 ± 1.55% (C30).

The cotton-reinforced series exhibited systematically higher absorption values than the cotton–polyester composites, attributable to the hydrophilic nature of the cellulosic fibers. The cotton–polyester reinforced composites demonstrated comparatively lower absorption values at equivalent fiber contents. CP05 (14.02 ± 0.61%) and CP10 (15.36 ± 0.68%) were statistically grouped with the legacy commercial products. At the highest fiber loading, CP30 exhibited a marked increase in absorption (30.38 ± 1.28%), indicative of a highly interconnected pore network established at high volume fractions.

The commercial cellulose fiber–cement ceiling sheets (CM05 and CM06) exhibited higher water absorption values (24.12 ± 1.06% and 32.64 ± 1.45%, respectively). Several experimental formulations, particularly CP05, CP10, and CP15, recorded statistically lower absorption values than these commercial references ($p < 0.05$).

3.1.5. Flexural Strength (Modulus of Rupture)

The flexural performance of the cementitious ceiling sheets, expressed as modulus of rupture (MOR), is presented in Figure 7, with statistical groupings summarized in Table 9. ANOVA confirmed that fiber reinforcement significantly influenced flexural performance ($p < 0.05$).

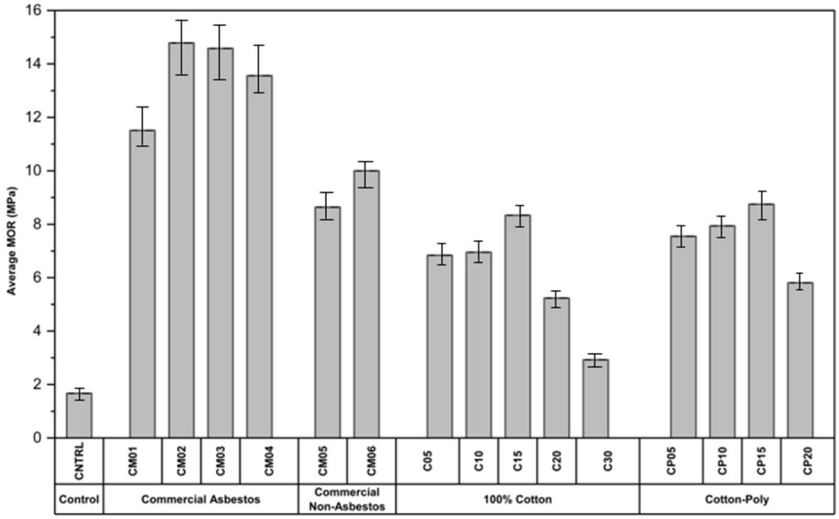

Figure 7. Flexural performance of textile-reinforced cementitious ceiling sheets relative to commercial benchmarks.

Table 9. Modulus of Rupture (MOR) Analysis with Statistical Grouping. Values represent Mean ± Standard Deviation (SD). Means sharing the same superscript letter are not statistically different ($p > 0.05$).

Sample Code	Reinforcement Type	Average MOR (MPa)
CNTRL	Control (Cement Only)	1.67 ± 0.13^{j}
C05	100% Cotton (5%)	6.84 ± 0.34^{fg}
C10	100% Cotton (10%)	6.95 ± 0.28^{fg}
C15	100% Cotton (15%)	8.34 ± 0.42^{d}
C20	100% Cotton (20%)	5.24 ± 0.31^{h}
C30	100% Cotton (30%)	2.93 ± 0.18^{i}
CP05	Cotton–Poly (5%)	7.55 ± 0.30^{ef}
CP10	Cotton–Poly (10%)	7.94 ± 0.24^{de}
CP15	Cotton–Poly (15%)	8.75 ± 0.35^{d}
CP20	Cotton–Poly (20%)	5.81 ± 0.41^{gh}
CP30	Cotton–Poly (30%)	5.92 ± 0.47^{gh}
CM01	Commercial Asbestos	11.51 ± 0.35^{b}
CM02	Commercial Asbestos	14.79 ± 0.59^{a}
CM03	Commercial Asbestos	14.58 ± 0.44^{a}
CM04	Commercial Asbestos	13.56 ± 0.54^{ab}
CM05	Commercial Non-Asbestos	8.64 ± 0.43^{d}
CM06	Commercial Non-Asbestos	10.00 ± 0.50^{c}

The cement-only control specimens exhibited the lowest MOR (1.67 ± 0.13 MPa), indicating the brittle behavior typical of unreinforced cementitious matrices. Upon fiber incorporation, all composite formulations demonstrated substantially enhanced flexural performance, attributed to the crack-arresting and bridging capabilities of the textile reinforcement.

For both reinforcement systems, an optimal performance threshold was observed at 15 wt.% fiber loading. Maximum MOR values were recorded at this threshold, with

CP15 achieving 8.75 ± 0.35 MPa and C15 achieving 8.34 ± 0.42 MPa. These specimens formed a common statistical group (Group d). Beyond 15 wt.%, a marked decline in flexural strength was observed. This reduction is attributed to excessive matrix dilution and fiber agglomeration, which compromise the fiber–matrix interfacial bond integrity. Consequently, the lowest MOR among the reinforced composites was recorded for the highly loaded C30 formulation (2.93 ± 0.18 MPa).

Benchmarking against commercial products reveals distinct performance tiers. The commercial cement fiber ceiling sheets of legacy formulation (CM01–CM04) exhibited the highest MOR values (11.51–14.79 MPa), reflective of their high-density, structural nature. In contrast, the commercial cellulose fiber–cement ceiling sheets (CM05 and CM06) displayed intermediate flexural performance (8.64–10.00 MPa). Crucially, statistical analysis confirms that the optimized experimental formulations (CP15 and C15) are statistically comparable ($p > 0.05$) to the commercial non-asbestos cellulose ceiling sheet (CM05). This demonstrates that the waste-valorized composites possess sufficient mechanical capacity for non-load-bearing ceiling applications, meeting the necessary industrial safety standards.

3.1.6. Dimensional Stability (Swelling)

While water absorption indicates porosity, dimensional stability is the critical parameter for durability. Table 10 presents the dimensional changes in the optimized composites after 24 h of water immersion (ISO 8336).

Table 10. Dimensional stability and swelling characteristics of optimized composites (24 h immersion).

Mix Code	Reinforcement	Thickness Swelling (%)	Length Expansion (%)	Width Expansion (%)
CNTRL	Cement Only	0.12 ± 0.05	0.02 ± 0.01	0.03 ± 0.01
CM02	Commercial Reference	0.45 ± 0.10	0.05 ± 0.02	0.06 ± 0.02
CP15	Cotton-Poly (15%)	1.35 ± 0.22	0.15 ± 0.04	0.18 ± 0.05
C15	100% Cotton (15%)	2.85 ± 0.45	0.32 ± 0.08	0.35 ± 0.09

The results presented in Table 10 confirm that the cementitious matrix effectively restrains the hygroscopic expansion of the textile reinforcement. Although the CP15 composite exhibited a higher water absorption capacity (21.6%) compared to the commercial reference (15.4%), its Thickness Swelling remained low at approximately 1.35%.

This behavior supports the hypothesis that while the porous network allows water ingress, the rigid cement binder prevents significant volume expansion. Notably, the Cotton–Polyester (CP15) formulation exhibited significantly lower swelling than the 100% Cotton (C15) equivalent (2.85%). This is attributed to the hydrophobic nature of the polyester fraction, which acts as a dimensionally stable skeleton within the fiber bundle, limiting the overall hygroscopic movement.

From a practical standpoint, the linear expansion (length and width) of the optimized CP15 composite was negligible (<0.20%). This confirms that the ceiling sheets possess sufficient dimensional stability to prevent warping or dislodging from standard suspension grids under humid tropical conditions.

3.2. Thermal Performance

Thermal Conductivity

The thermal conductivity of the textile-reinforced cementitious ceiling sheets, benchmarked against commercial cement fiber ceiling sheets, is presented in Figure 8, with statistical groupings summarized in Table 11. ANOVA confirmed that both reinforce-

ment type and fiber loading had a statistically significant effect on thermal conductivity ($p < 0.05$).

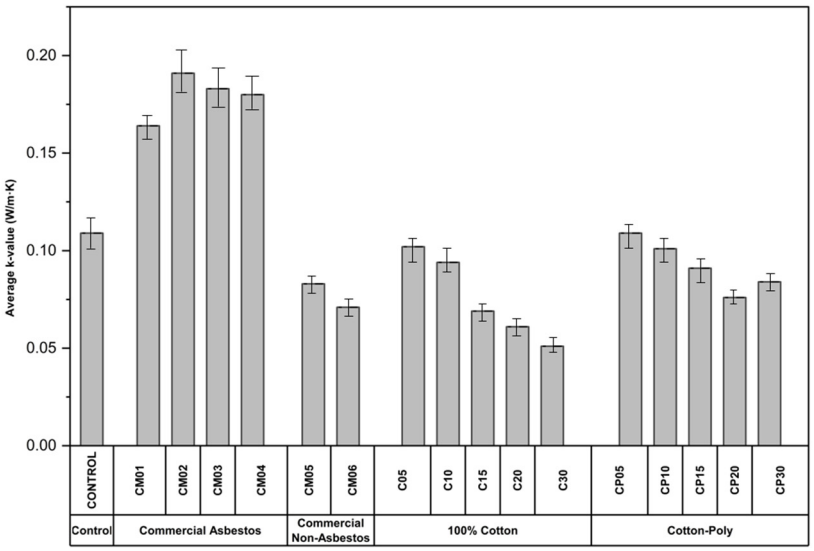

Figure 8. Thermal conductivity of textile-reinforced cementitious ceiling sheets relative to commercial products.

Table 11. Thermal Conductivity Analysis with Statistical Grouping. Values represent Mean ± Standard Deviation (SD). Means sharing the same superscript letter are not statistically different ($p > 0.05$).

Sample Code	Reinforcement Type	Average k-Value (W/m·K)
CONTROL	Control (Cement Only)	0.109 ± 0.005^{c}
C05	100% Cotton (5%)	0.102 ± 0.004^{c}
C10	100% Cotton (10%)	0.094 ± 0.003^{d}
C15	100% Cotton (15%)	0.069 ± 0.003^{f}
C20	100% Cotton (20%)	0.061 ± 0.003^{f}
C30	100% Cotton (30%)	0.051 ± 0.003^{g}
CP05	Cotton–Poly (5%)	0.109 ± 0.004^{c}
CP10	Cotton–Poly (10%)	0.101 ± 0.005^{d}
CP15	Cotton–Poly (15%)	0.091 ± 0.004^{d}
CP20	Cotton–Poly (20%)	0.076 ± 0.003^{e}
CP30	Cotton–Poly (30%)	0.084 ± 0.003^{de}
CM01	Commercial Asbestos	0.164 ± 0.006^{b}
CM02	Commercial Asbestos	0.191 ± 0.009^{a}
CM03	Commercial Asbestos	0.183 ± 0.007^{a}
CM04	Commercial Asbestos	0.180 ± 0.008^{a}
CM05	Commercial Non-Asbestos	0.083 ± 0.004^{e}
CM06	Commercial Non-Asbestos	0.071 ± 0.003^{ef}

The commercial cement fiber ceiling sheets of legacy formulation (CM01–CM04) exhibited the highest thermal conductivity values, ranging from 0.164 to 0.191 W/m·K, occupying the upper statistical groups (Groups a and b). This behavior is characteristic of their high-density, compacted matrices which facilitate conductive heat transfer. The

unreinforced cement control specimens showed a significantly lower thermal conductivity of 0.109 ± 0.005 W/m·K.

Progressive reductions in thermal conductivity were observed with increasing textile fiber incorporation. This trend validates the hypothesis that fiber incorporation disrupts conductive heat transfer pathways through two mechanisms: (1) the lower intrinsic thermal conductivity of the polymer/cellulose fibers compared to the cement matrix, and (2) the creation of interfacial air voids and increased porosity induced by the fiber "spring-back" effect.

Among the cotton–polyester composites, a monotonic decrease was observed, reaching a significant reduction at 20 wt.% fiber loading (CP20) with a value of 0.076 ± 0.003 W/m·K. This represents a substantial improvement in thermal insulation compared to the legacy commercial products. The cotton-reinforced composites exhibited the lowest thermal conductivity values overall. Specifically, C15 achieved 0.069 ± 0.003 W/m·K, and with further fiber loading, C30 reached a minimum value of 0.051 ± 0.003 W/m·K.

Benchmarking against modern alternatives, the commercial cellulose fiber–cement ceiling sheets exhibited intermediate thermal conductivity values (0.083 ± 0.004 W/m·K for CM05 and 0.071 ± 0.003 W/m·K for CM06). Crucially, the experimental formulations CP20 and C15 were statistically comparable ($p > 0.05$) to these commercial references, confirming that the waste-valorized composites achieve the thermal insulation standards required for modern ceiling applications.

3.3. Microstructural Analysis

The microstructural morphology of the fractured surfaces was examined to elucidate the mechanisms governing the physical and mechanical behavior of the composites. The SEM analysis focused on fiber dispersion, the integrity of the fiber–matrix Interfacial Transition Zone (ITZ), and the pore structure evolution.

3.3.1. Morphology of Cotton-Reinforced Composites (C15)

Micrographs of the C15 (15 wt.% Cotton) formulation reveal the characteristic ribbon-like morphology of the processed cotton fibers, which appear flattened and twisted within the cementitious matrix (Figure 9a). While the fibers are generally well-distributed, localized clustering is observed, corresponding to the "spring-back" regions where the elastic recovery of the fiber bundles inhibited full matrix penetration during compaction.

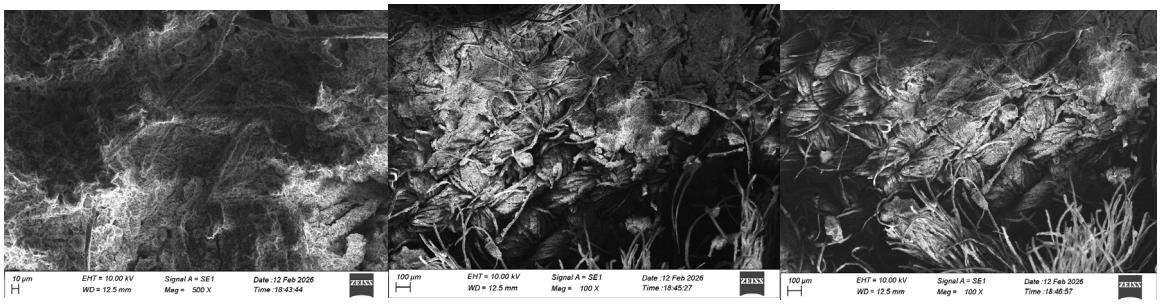

(**a**) (**b**) (**c**)

Figure 9. SEM micrographs of C15 (15 wt.% Cotton) composite: (**a**) Fiber distribution showing flattened, twisted ribbon morphology; (**b**,**c**) Interfacial Transition Zone (ITZ) exhibiting debonding gaps and hollow fiber lumens.

A defining feature observed at higher magnification is the presence of interfacial micro-gaps (debonding) between the fiber surface and the surrounding cement hydration products (Figure 9b). This debonding is attributed to the dimensional mismatch during the

curing phase: the hydrophilic cotton fibers absorb mix water and swell during casting, but subsequently shrink as the cement consumes water for hydration. This shrinkage leaves behind a distinct gap at the ITZ, which explains the reduced specific strength observed in the monoculture cotton samples compared to the control.

Crucially, the micrographs clearly identify the hollow lumen structure of the cotton fibers. Many fibers exhibit a collapsed or tubular cross-section. These hollow cores, combined with the interfacial shrinkage gaps, act as intrinsic air traps. This visual evidence provides the microstructural basis for the thermal conductivity results (Section 3.2), confirming that the high insulation value (<0.35 W/m·K) is derived from both the macroscopic matrix porosity and the intra-fiber voids of the reinforcement.

3.3.2. Morphology of Hybrid Composites (CP20)

The CP20 (20 wt.% Cotton–Polyester) formulation displays a complex hybrid microstructure (Figure 10a). The polyester fibers are easily distinguishable as smooth, cylindrical filaments that maintain their circular cross-section, contrasting sharply with the irregular, flattened cotton ribbons.

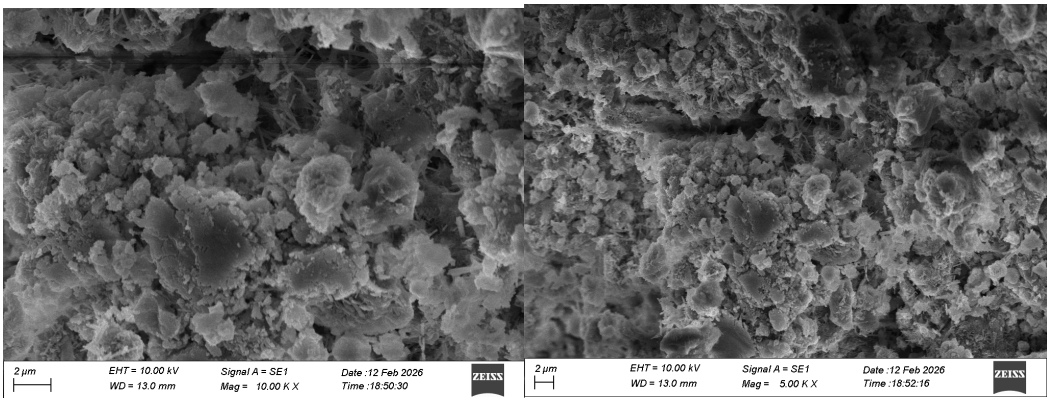

(**a**) (**b**)

Figure 10. SEM micrographs of CP20 (Cotton–Polyester) composite: (**a**) Hybrid network distinguishing flattened cotton and cylindrical polyester fibers; (**b**) Smooth polyester fiber surface indicating frictional pull-out failure mode.

The fiber–matrix interface for the polyester phase appears "clean," with minimal encrustation of C-S-H gel or hydration products (Figure 10b). This indicates a primarily frictional bond rather than a chemical one, consistent with the hydrophobic nature of the polymer. The fracture surfaces exhibit numerous smooth cylindrical sockets, confirming that fiber pull-out is the dominant failure mechanism for the polyester fraction.

Unlike the cotton fibers, the polyester filaments do not show significant shrinkage gaps at the interface. This suggests that the polyester phase acts as a dimensionally stable scaffold within the hybrid network. While the cotton fibers swell and shrink, the inert polyester fibers bridge the resulting micro-cracks and restrict the overall macroscopic expansion. This microstructural observation directly validates the dimensional stability results (Section 3.1.2), where the CP formulations exhibited significantly lower swelling than the pure cotton equivalents despite high porosity.

4. Discussion

The results of this study demonstrate that the incorporation of post-industrial textile waste induces fundamental modifications to the physical, mechanical, and thermal behavior of cementitious ceiling sheets. These changes arise from coupled effects of cement matrix dilution, fiber–matrix interfacial behavior, and microstructural porosity evolution

under hydraulic pressing. Rather than yielding monotonic improvements across all performance metrics, textile fiber incorporation introduces a controlled performance trade-off that must be optimized to achieve technically and industrially viable non-load-bearing ceiling elements.

4.1. Microstructural Evolution and Process Dynamics

The results demonstrate that incorporation of post-industrial textile waste fundamentally alters the physical, mechanical, and thermal behavior of cementitious ceiling sheets. These modifications arise from coupled mechanisms involving matrix dilution, fiber–matrix interfacial interactions, and porosity evolution under hydraulic pressing. Rather than producing monotonic performance enhancement, fiber incorporation introduces a controlled trade-off that must be optimized to achieve technically and industrially viable non-load-bearing ceiling elements.

The progressive reduction in apparent density with increasing fiber content is governed by two concurrent mechanisms: material substitution and microstructural expansion. First, partial replacement of the high-density cementitious matrix with lower-density textile fibers directly decreases bulk density. Second, elastic recovery ("spring-back") of fibers following compaction limits full matrix consolidation, amplifying porosity development.

The preliminary optimization study (Section 3.1.1) confirms that this microstructural evolution is strongly dependent on applied processing energy. During pressing, textile fibers undergo temporary deformation; upon pressure release, partial elastic recovery generates distributed micro-voids within the cementitious matrix. This spring-back phenomenon becomes increasingly pronounced at higher fiber loadings, consistent with the measured increases in specimen thickness and open pore volume reported in Section 3.1.2 [23,47–49].

Critically, the selection of 2.0 MPa as the compaction pressure represents a deliberate processing threshold. Although higher pressures (e.g., 2.5 MPa) could reduce spring-back and produce thinner sheets, experimental observations indicate that excessive compaction causes localized crushing of hollow fiber lumens. Because thermal insulation performance relies on air entrapment within these lumens, increased compaction would compromise the material's primary functional advantage. Thus, the thickness increase observed at 2.0 MPa should not be interpreted as a manufacturing defect, but rather as a necessary structural consequence of preserving a thermally functional porous architecture.

4.2. Structural Loading and System Compatibility

For ceiling applications, areal density (kg/m^2) governs structural compatibility, as it determines the dead load imposed on suspension systems. Interpreting density solely through bulk values (g/cm^3) can be misleading, particularly since the experimental sheets exhibit increased thickness due to spring-back.

Based on measured physical properties (Tables 6 and 7), the optimized CP15 composite exhibits an areal density of approximately 10.84 kg/m^2 (1.63 g/cm^3 × 6.65 mm). Although this represents a 61.8% increase relative to thin legacy asbestos-cement sheets (6.70 kg/m^2), benchmarking must consider contemporary safe alternatives. Standard 12.5 mm gypsum ceiling boards typically impose a dead load of 9.0–10.5 kg/m^2. The CP15 composite falls within this operational range, confirming compatibility with conventional gypsum-grade suspension grids.

This finding is industrially significant. It demonstrates that, despite increased thickness, the proposed composite does not require specialized heavy-duty framing. Therefore, the enhanced thermal performance is achieved without compromising structural system integration or increasing installation complexity.

4.3. Thermal Conductivity Mechanisms

Thermal conductivity trends directly reflect the microstructural transformations described in Section 4.1. The substantial reduction in thermal conductivity observed in textile-reinforced composites arises from the combined influence of intrinsic fiber morphology and increased pore volume.

SEM analysis (Section 3.3) provides mechanistic evidence for this behavior. Processed cotton fibers retain their hollow lumen structure and exhibit localized interfacial debonding gaps resulting from shrinkage (Figure 9b). These features establish a hierarchical double-porosity system comprising:

(1) macro-porosity generated by fiber spring-back;
(2) micro-porosity associated with hollow fiber lumens.

Air entrapped within these discontinuities disrupts conductive heat transfer pathways through the cementitious matrix, thereby significantly lowering effective thermal conductivity (<0.10 W/m·K) [50–52]. The hollow lumens act as intrinsic insulating micro-chambers, while macro-voids further increase tortuosity of heat flow.

Although polyester fibers lack internal lumens, they contribute to thermal resistance by interrupting continuous cementitious conduction pathways. Due to comparatively weaker fiber–matrix adhesion, polyester fibers promote interfacial air gap formation, further enhancing thermal impedance. At elevated fiber contents, additional micro-void generation through elastic recovery increases air entrapment, thereby amplifying insulation performance [53–55].

Collectively, these mechanisms explain the observed 40–50% reduction in thermal conductivity relative to legacy commercial cement fiber ceiling sheets, confirming that porosity engineering, rather than simple material substitution, is the dominant thermal efficiency driver.

4.4. Moisture Dynamics and Dimensional Stability

Water absorption behavior provides critical insight into the interplay between fiber chemistry and pore connectivity. The progressive increase in moisture uptake with increasing fiber content is primarily attributed to the hydrophilic nature of cotton fibers, which contain abundant hydroxyl functional groups capable of hydrogen bonding with water molecules [56,57]. Additionally, the intrinsic lumen structure of cotton fibers facilitates capillary transport, particularly at higher fiber loadings (e.g., CP30), where interconnected pore networks become more pronounced [58].

Importantly, a distinction must be made between volumetric absorption (porosity-driven water uptake) and dimensional swelling (macroscopic expansion). Durability results (Table 10) demonstrate a clear decoupling between these parameters. Although the CP15 composite exhibited relatively high water absorption (~21%), its thickness swelling remained limited to 1.35%. This behavior is governed by a matrix-confinement mechanism, wherein the rigid cementitious matrix imposes internal restraint that suppresses fiber expansion at the macroscale.

SEM observations of the hybrid CP20 composite (Figure 10) further elucidate the role of fiber synergy. Unlike cotton fibers, which exhibited localized shrinkage-induced debonding, the hydrophobic polyester fibers maintained a stable frictional interface with the cement paste. These fibers function as a dimensionally stable scaffold, bridging microcracks and restricting moisture-induced deformation [59,60]. Such behavior is particularly advantageous for ceiling applications in humid tropical environments, where resistance to moisture-driven degradation is essential for long-term serviceability [61–63].

4.5. Mechanical Efficiency and Failure Modes

Mechanical performance reveals a reinforcement threshold governed by fiber dispersion and interfacial efficiency. At low to intermediate fiber loadings, fibers are sufficiently dispersed to enable effective crack-bridging, thereby enhancing modulus of rupture relative to unreinforced matrices [48,64–66]. In this regime, stress transfer across the fiber–matrix interface is optimized without excessive porosity or agglomeration.

SEM-based failure analysis clarifies the governing mechanisms. The C15 (100% cotton) samples exhibited distinct interfacial gaps (Figure 9b), which act as stress concentrators and promote premature crack initiation. In contrast, the hybrid CP20 samples displayed clear evidence of fiber pull-out (Figure 10b), indicating a toughening mechanism dominated by frictional energy dissipation. Although chemical bonding between polyester fibers and the cement matrix is limited, the frictional anchorage is sufficient to preserve structural continuity during crack propagation.

Beyond the optimal 15 wt.% threshold, excessive fiber incorporation promotes agglomeration and increases interfacial defects, reducing effective stress transfer and resulting in diminished flexural performance [67–69]. This confirms that mechanical efficiency is controlled not solely by fiber content, but by the balance between dispersion quality, interfacial interaction, and pore architecture.

4.6. Comparative Analysis and Industrial Relevance

The inverse relationship observed between thermal and mechanical performance underscores an inherent optimization challenge. Elevated fiber contents enhance thermal resistance through increased porosity but compromise mechanical integrity. Conversely, lower fiber contents maintain structural strength but provide limited thermal insulation benefit [70–72].

Among the evaluated formulations, CP15 achieves the most favorable performance balance. It attains a flexural strength of approximately 8.75 MPa—exceeding ISO 8336 Category C [2], Class 2 requirements—while reducing thermal conductivity by approximately 40–50% relative to commercial cement fiber benchmarks. Comparative assessment highlights the practical relevance of this balance: conventional cement fiber sheets provide adequate strength but limited thermal performance, whereas cellulose-based sheets often suffer from moisture sensitivity. The optimized cotton–polyester hybrid composites demonstrate a balanced property profile that integrates thermal efficiency, mechanical compliance, and dimensional stability [20,73,74].

From an industrial perspective, the direct utilization of post-industrial textile waste aligns with circular economy objectives. The fabrication process relies on conventional cement processing techniques, suggesting that large-scale adoption could be achieved with minimal modification to existing production infrastructure [24,75,76]. By elucidating the mechanisms governing density reduction, thermal conductivity modification, interfacial performance, and moisture stability, this study establishes a mechanistic framework for optimizing textile-reinforced cementitious composites in sustainable ceiling and partition applications.

5. Conclusions

This study systematically demonstrated the feasibility of valorizing post-industrial textile waste (100% cotton and cotton–polyester blends) as functional reinforcement in cementitious ceiling sheets. The results confirm that controlled processing conditions fundamentally govern composite performance. In particular, a hydraulic compaction pressure of 2.0 MPa was identified as a critical process threshold. At this pressure, the fibrous network undergoes controlled viscoelastic recovery (“spring-back”) upon demolding, in-

creasing the final sheet thickness by approximately 60–66% relative to the mold depth. Rather than constituting a manufacturing defect, this phenomenon generates a hierarchical double-porosity architecture composed of macro-voids formed by elastic recovery and micro-voids associated with hollow fiber lumens, which collectively underpin the material's thermal functionality.

The induced porosity substantially enhanced thermal insulation without compromising structural reliability. The optimized CP15 (cotton–polyester) composite achieved a thermal conductivity of 0.091 W/m·K, representing an approximate 50% reduction compared to conventional cement fiber ceiling sheets. Mechanical evaluation identified an optimal reinforcement threshold at 15 wt.% fiber loading, where the CP15 formulation attained a Modulus of Rupture (MOR) of 8.75 MPa, exceeding the ISO 8336 Category C, Class 2 requirement (7 MPa) for non-load-bearing applications. Although the spring-back effect increased sheet thickness, the resulting areal density (10.84 kg/m^2) remains comparable to standard 12.5 mm gypsum boards (9.0–10.5 kg/m^2), confirming compatibility with conventional suspended ceiling grid systems and eliminating the need for specialized structural reinforcement.

From a durability perspective, a key mechanistic insight was the decoupling between water absorption and dimensional swelling. Despite relatively high moisture uptake (~21%), thickness swelling of the optimized CP15 hybrid composite was limited to 1.35%. Scanning Electron Microscopy (SEM) indicates that the hydrophobic polyester scaffold provides frictional anchorage and microcrack-bridging capacity, thereby constraining the hygroscopic expansion of the hydrophilic cotton fraction. This hybrid reinforcement strategy effectively mitigates the durability limitations commonly associated with bio-fiber composites under humid tropical conditions.

Collectively, these findings validate a direct-valorization pathway utilizing textile waste in its native industrial state, thereby reducing embodied energy by eliminating chemical scouring processes. The study demonstrates that high-performance, thermally efficient, and structurally compliant circular construction materials can be engineered from untreated industrial by-products.

Limitations and Future Work

While the present work establishes physical, mechanical, and thermal feasibility, further investigation is required prior to large-scale commercialization. Given the combustible nature of cellulosic and polymeric textile constituents, fire performance and flame spread characteristics should be evaluated (e.g., BS 476 [77] or ASTM E84 [78]) to determine appropriate fire-retardant strategies for indoor applications. Additionally, the highly porous architecture suggests potential acoustic functionality; future studies should quantify the Noise Reduction Coefficient (NRC) to assess suitability as a dual-purpose thermal–acoustic ceiling system. Finally, a comprehensive Life Cycle Assessment (LCA) is recommended to quantify embodied carbon reduction and broader environmental impacts relative to conventional gypsum and fiber–cement alternatives, thereby providing holistic validation of the proposed circular economy approach.

Author Contributions: Conceptualization, C.A.D., K.V.F., U.S.W.G. and R.U.H.; Methodology, C.A.D., K.V.F., V.M.S., S.M.J. and G.N.G.; Validation, C.A.D., U.S.W.G. and R.U.H.; Formal analysis, C.A.D.; Investigation, C.A.D. and K.V.F.; Resources, U.S.W.G. and R.U.H.; Data curation, C.A.D., K.V.F., V.M.S., S.M.J., R.H.H. and G.N.G.; Writing—original draft preparation, C.A.D. and K.V.F.; Writing—review and editing, D.D., U.S.W.G. and R.U.H.; Visualization, C.A.D., G.N.G. and R.H.H.; Supervision, D.D., U.S.W.G. and R.U.H.; Project administration, U.S.W.G. and R.U.H.; Funding acquisition, D.D., U.S.W.G. and R.U.H. All authors have read and agreed to the published version of the manuscript.

Funding: The Article Processing Charge (APC) was funded by the Sri Lanka Institute of Information Technology (SLIIT).

Data Availability Statement: The original contributions presented in this study are included in the article. Further inquiries can be directed to the corresponding author.

Acknowledgments: The authors wish to acknowledge the Kalama Mithuro organization for their support during this research. We also extend our gratitude to Celsius Solutions (Pvt) Ltd. and Hayleys Fabric PLC for providing the essential raw materials that enabled us to carry out our experimental work successfully. Furthermore, we thank technical officers W.B.U. Rukma, M.T.M.R. Jayaweera, P.S.S. Perera, M.A.P.C. Gunawardena, D.M.B. Wickramasinghe, and T.P.D.G.I. Yohan for their technical assistance, as well as W.J. Shantha, A.W.A.D.B. Abeykoon, and L.H.K. Chandana for their support in the laboratory.

Conflicts of Interest: The authors declare no conflicts of interest.

References

1. Weber, H.; Sciubba, J.D. The Effect of Population Growth on the Environment: Evidence from European Regions. *Eur. J. Popul.* **2019**, *35*, 379–402. [CrossRef]
2. Dodangodage, C.A.; Premarathne, H.; Kasturiarachchi, J.C.; Perera, T.A.; Rajapakshe, D.; Halwatura, R.U. Algae-Based Protective Coatings for Sustainable Infrastructure: A Novel Framework Linking Material Chemistry, Techno-Economics, and Environmental Functionality. *Phycology* **2025**, *5*, 84. [CrossRef]
3. Gautam, M.; Agrawal, M. Greenhouse Gas Emissions from Municipal Solid Waste Management: A Review of Global Scenario. In *Carbon Footprint Case Studies: Municipal Solid Waste Management, Sustainable Road Transport and Carbon Sequestration*; Muthu, S.S., Ed.; Springer: Singapore, 2021; pp. 123–160. [CrossRef]
4. Abtew, M.A.; Atalie, D.; Dejene, B.K. Recycling of cotton textile waste: Technological process, applications, and sustainability within a circular economy. *J. Ind. Text.* **2025**, *55*, 15280837251348664. [CrossRef]
5. Wojnowska-Baryła, I.; Bernat, K.; Zaborowska, M.; Kulikowska, D. The Growing Problem of Textile Waste Generation—The Current State of Textile Waste Management. *Energies* **2024**, *17*, 1528. [CrossRef]
6. Baloyi, R.B.; Gbadeyan, O.J.; Sithole, B.; Chunilall, V. Recent advances in recycling technologies for waste textile fabrics: A review. *Text. Res. J.* **2024**, *94*, 508–529. [CrossRef]
7. Hossain, M.I.; Zhang, Y.; Haque, A.N.M.A.; Naebe, M. Fibrous Microplastics Release from Textile Production Phases: A Brief Review of Current Challenges and Applied Research Directions. *Materials* **2025**, *18*, 2513. [CrossRef]
8. Rashid, M.E.; Khan, M.R.; Haque, R.U.; Hasanuzzaman, M. Challenges of textile waste composite products and its prospects of recycling. *J. Mater. Cycles Waste Manag.* **2023**, *25*, 1267–1287. [CrossRef]
9. Lglm, E.; Alwis, A. Waste flow analysis in textile and apparel sector, A case study of textile and apparel wet processing industries in Sri Lanka. *J. Res. Technol. Eng.* **2021**, *2*, 1–8.
10. Edirisinghe, L.G.L.M.; Wijayasundara, M.; De Alwis, A.A.P. Waste Generation and Characteristics in Sri Lankan Textile and Apparel Sector: Case Study of the Biyagama Industrial Export Processing Zone, Sri Lanka. *Nat. Environ. Pollut. Technol.* **2022**, *21*, 697–702. [CrossRef]
11. Dodangodage, C.A.; Kasturiarachchi, J.C.; Wijesekara, I.A.; Perera, T.A.; Rajapakshe, D.; Halwatura, R. Integrated Microalgal–Aquaponic Systems for Enhanced Water Treatment and Food Security: A Critical Review of Recent Advances in Process Integration and Resource Recovery. *Phycology* **2026**, *6*, 14. [CrossRef]
12. Dodangodage, C.A.; Gamage, G.N.; Fernando, K.V.; Kasturiarachchi, J.C.; Perera, T.A.; Rajapakshe, S.D.; Halwatura, R.U. Production of Carbohydrate-Rich *Chlorella* sp. Biomass Using Clarified Aquaponics Effluent for Bioethanol Feedstock Applications. 2025. Available online: https://doi.org/10.20944/preprints202512.1475.v1 (accessed on 16 December 2025).
13. Dodangodage, C.A.; Gamage, G.N.; Wijesekara, I.A.; Kasturiarachchi, J.C.; Perera, T.A.; Rajapakshe, D.; Halwatura, R.U. Valorization of Canteen Wastewater Through Optimized *Spirulina Platensis* Cultivation for Enhanced Carotenoid Production and Nutrient Removal. *Phycology* **2026**, *6*, 15. [CrossRef]
14. Dodangodage, C.A.; Premarathne, H.; Nadeniya, C.; Nethsara Gamage, G.; Halwatura, R.H.; Kasturiarachchi, J.C.; Perera, T.A.; Rajapakshe, D.; Halwatura, R.U. Mixotrophic Cultivation of *Desmodesmus* sp. in Matured Compost Leachate: Growth Kinetics, Nutrient Removal, and Stress-Induced Lipid Production. 2025. Available online: https://doi.org/10.20944/preprints202601.1662.v1 (accessed on 16 January 2026).
15. Alves, D.I.; Barreiros, M.; Fangueiro, R.; Ferreira, D.P. Valorization of textile waste: Non-woven structures and composites. *Front. Environ. Sci.* **2024**, *12*, 1365162. [CrossRef]

16. Papamichael, I.; Voukkali, I.; Economou, F.; Loizia, P.; Demetriou, G.; Esposito, M.; Naddeo, V.; Liscio, M.C.; Sospiro, P.; Zorpas, A.A. Mobilisation of textile waste to recover high added value products and energy for the transition to circular economy. *Environ. Res.* **2024**, *242*, 117716. [CrossRef] [PubMed]
17. Shirvanimoghaddam, K.; Motamed, B.; Ramakrishna, S.; Naebe, M. Death by waste: Fashion and textile circular economy case. *Sci. Total Environ.* **2020**, *718*, 137317. [CrossRef] [PubMed]
18. Gil, L.K.T.; Valdelamar Martínez, D.; Franco, K.B.; Arrieta Pastrana, A.; Saba, M. Mapping roof coverings of asbestos-cement, the first step to control the technical condition/threat and establish priorities for replacement in developing countries. *Heliyon* **2024**, *10*, e37522. [CrossRef]
19. Deix, K.; Huber, C.; Gogic, J. Efficiency of Alternative Reinforcement Methods for Wooden Ceilings and Their Ecological Aspects. *Materials* **2025**, *18*, 2032. [CrossRef]
20. Onyeaju, M.C.; Osarolube, E.; Chukwuocha, E.O.; Ekuma, C.E.; Omasheye, G.A.J. Comparison of the thermal properties of asbestos and polyvinylchloride (PVC) ceiling sheets. *Mater. Sci. Appl.* **2012**, *3*, 240–244. [CrossRef]
21. Kottek, M.; Yuen, M.L. Public health risks from asbestos cement roofing. *Am. J. Ind. Med.* **2022**, *65*, 157–161. [CrossRef]
22. Tonoli, G.H.D.; dos Santos, S.F.; Rabi, J.A.; dos Santos, W.N.; Savastano Junior, H. Thermal performance of sisal fiber-cement roofing tiles for rural constructions. *Sci. Agric.* **2011**, *68*, 1–7. [CrossRef]
23. Sadrolodabaee, P.; Claramunt, J.; Ardanuy, M.; de la Fuente, A. A textile waste fiber-reinforced cement composite: Comparison between short random fiber and textile reinforcement. *Materials* **2021**, *14*, 3742. [CrossRef]
24. Baričević, A.; Didulica, K.; Smrkić, M.F.; Jelčić Rukavina, M. Cementitious composites reinforced with waste fibres from the production of high-quality construction textiles. *Materials* **2022**, *15*, 1611. [CrossRef]
25. Yao, Y.; Xu, G.; Wu, M.; Zhao, M. Exploring the influence of cement and cement hydration products on strength and interfacial adhesion in emulsified cold recycled mixture: A molecular dynamics and experimental investigation. *Constr. Build. Mater.* **2023**, *409*, 134050. [CrossRef]
26. Chen, X.; Memon, H.A.; Wang, Y.; Marriam, I.; Tebyetekerwa, M. Circular Economy and Sustainability of the Clothing and Textile Industry. *Mater. Circ. Econ.* **2021**, *3*, 12. [CrossRef]
27. Anas, M.S.; Faheem, M.; Mikucioniene, D. Challenges and Limitations in Recycling of Post-Consumer Cotton Denim Waste into New Textiles. *J. Nat. Fibers* **2025**, *22*, 2570080. [CrossRef]
28. Leenders, N.; van Klink, G.P.M.; Gruter, G.J.M. Towards polycotton waste valorisation: Depolymerisation of cotton to glucose with polyester preservation. *RSC Sustain.* **2025**, *3*, 3863–3882. [CrossRef]
29. Yan, L.; Kasal, B.; Huang, L. A review of recent research on the use of cellulosic fibres, their fibre fabric reinforced cementitious, geo-polymer and polymer composites in civil engineering. *Compos. Part. B Eng.* **2016**, *92*, 94–132. [CrossRef]
30. Liu, J.; Lv, C. Research Progress on Durability of Cellulose Fiber-Reinforced Cement-Based Composites. *Int. J. Polym. Sci.* **2021**, *2021*, 1014531. [CrossRef]
31. Zou, Y.; Reddy, N.; Yang, Y. Reusing polyester/cotton blend fabrics for composites. *Compos. Part. B Eng.* **2011**, *42*, 763–770. [CrossRef]
32. Kahoush, M.; Kadi, N. Towards sustainable textile sector: Fractionation and separation of cotton/polyester fibers from blended textile waste. *Sustain. Mater. Technol.* **2022**, *34*, e00513. [CrossRef]
33. Udawattha, C.; Galabada, H.; Halwatura, R. Mud concrete paving block for pedestrian pavements. *Case Stud. Constr. Mater.* **2017**, *7*, 249–262. [CrossRef]
34. Chandima, A.M.B.; Guluwita, S.P. Effects of Carbon Black and Graphene Oxide Additions on Properties of Ordinary Portland Cement Composite. In *ICSBE 2020*; Dissanayake, R., Mendis, P., Weerasekera, K., De Silva, S., Fernando, S., Eds.; Springer: Singapore, 2022; pp. 385–397. [CrossRef]
35. Peña-Pichardo, P.; Martínez-Barrera, G.; Martínez-López, M.; Ureña-Núñez, F.; dos Reis, J.M.L. Recovery of cotton fibers from waste Blue-Jeans and its use in polyester concrete. *Constr. Build. Mater.* **2018**, *177*, 409–416. [CrossRef]
36. Babaarslan, O.; Shahid, M.A.; Okyay, N. Investigation of the performance of cotton/polyester blend in different yarn structures. *AUTEX Res. J.* **2023**, *23*, 370–380. [CrossRef]
37. Cook, D.J.; Pama, R.P.; Weerasingle, H.L.S.D. Coir fibre reinforced cement as a low cost roofing material. *Build. Environ.* **1978**, *13*, 193–198. [CrossRef]
38. Agopyan, V.; Savastano, H.; John, V.M.; Cincotto, M.A. Developments on vegetable fibre–cement based materials in São Paulo, Brazil: An overview. *Cem. Concr. Compos.* **2005**, *27*, 527–536. [CrossRef]
39. Chen, X.; Wu, S. Influence of water-to-cement ratio and curing period on pore structure of cement mortar. *Constr. Build. Mater.* **2013**, *38*, 804–812. [CrossRef]
40. El Hamri, A.; Mouhib, Y.; Ourmiche, A.; Chigr, M.; El Mansouri, N.E. Study of the Effect of Cedar Sawdust Content on Physical and Mechanical Properties of Cement Boards. *Molecules* **2024**, *29*, 4399. [CrossRef]
41. Guo, G.; Zhao, S.; Wen, D.; Zhang, G.; Liu, L. Experimental study on the influence of different curing methods on the performance of concrete. *J. Meas. Eng.* **2025**, *13*, 25–34. [CrossRef]

42. Bodnarova, L.; Hosko, M.; Martinec, P. Methods of testing the properties of fibre-cement composites. *IOP Conf. Ser. Mater. Sci. Eng.* **2018**, *385*, 012005.
43. *ASTM C1185*; Standard Test Methods for Sampling and Testing Non-Asbestos Fiber-Cement Flat Sheet, Roofing and Siding Shingles, and Clapboards. ASTM International: West Conshohocken, PA, USA, 1999.
44. Ranachowski, Z.; Schabowicz, K. *The Fabrication, Testing and Application of Fibre Cement Boards*; Cambridge Scholars Publishing: Newcastle upon Tyne, UK, 2018.
45. *ASTM C518-21*; Standard Test Method for Steady-State Thermal Transmission Properties by Means of the Heat Flow Meter Apparatus. ASTM International: West Conshohocken, PA, USA, 2021.
46. Knězek, I.J.; Modrý, I.S. Proposal for Prognosis of Composite Materials Durability on the Basis of Accelerated Tests. In *Application of Codes, Design and Regulations: Proceedings of the International Conference Held at the University of Dundee, Scotland, UK, 5–7 July 2005*; ICE Publishing: London, UK, 2005; pp. 255–262. [CrossRef]
47. Wei, X.; Deng, Z.; Fu, X.; Zhang, H.; Wang, M.; Wang, L.; Zheng, Y.; Zhi, S. Compressed springback deformation characteristics of Xinjiang machine-harvested seed cotton. *Ind. Crops Prod.* **2025**, *225*, 120498. [CrossRef]
48. Grings, K.J.O.; Carneiro Ribeiro, F.R.; Junior, D.V.A.; de Azevedo, A.R.G.; Kulakowski, M.P. Evaluation of Light Cementitious Matrix with Composite Textile Reinforcement from Garment Waste. *Materials* **2023**, *16*, 733. [CrossRef]
49. Styks, J.; Knapczyk, A.; Łapczyńska-Kordon, B. Effect of compaction pressure and moisture content on post-agglomeration elastic springback of pellets. *Materials* **2021**, *14*, 879. [CrossRef]
50. Shalwan, A.; Alajmi, A.; Yousif, B.F. Theoretical Study of the Effect of Fibre Porosity on the Heat Conductivity of Reinforced Gypsum Composite Material. *Polymers* **2022**, *14*, 3973. [CrossRef]
51. El-Hage, Y.; Hind, S.; Robitaille, F. Thermal conductivity of textile reinforcements for composites. *J. Text. Fibrous Mater.* **2018**, *1*, 2515221117751154. [CrossRef]
52. Darda, M.A.; Bhuiyan, M.A.R.; Bari, M.A.; Islam, S.; Hossen, M.J. Mechanically robust and thermally insulating natural cotton fiber-reinforced biocomposite panels for structural applications. *RSC Adv.* **2025**, *15*, 9534–9545. [CrossRef] [PubMed]
53. Yang, T.; Xiong, X.; Petrů, M.; Tan, X.; Kaneko, H.; Militký, J.; Sakuma, A. Theoretical and experimental studies on thermal properties of polyester nonwoven fibrous material. *Materials* **2020**, *13*, 2882. [CrossRef] [PubMed]
54. Mahan, H.M.; Katawy, A.; Shabeeb, O.A.; Alrubaiy, A.A.A.G. Analyzing thermal insulation of concrete polymer by adding mineral wool. *Adv. Sci. Technol. Res. J.* **2025**, *19*, 430–439. [CrossRef]
55. Yang, P.; Wu, Y.; Wang, K.; Zheng, X.; Wan, J.; Wu, K.; Shi, J.; Hong, P.; Yang, L. Intrinsic Thermal Conductivity of Polyesters with Flexible Segments in Main Chains. *J. Phys. Chem. C* **2025**, *129*, 2788–2796. [CrossRef]
56. Simon, M.; Fulchiron, R.; Gouanvé, F. Water Sorption and Mechanical Properties of Cellulosic Derivative Fibers. *Polymers* **2022**, *14*, 2836. [CrossRef]
57. Sahu, P.; Gupta, M.K. Water absorption behavior of cellulosic fibres polymer composites: A review on its effects and remedies. *J. Ind. Text.* **2022**, *51*, 7480S–7512S. [CrossRef]
58. Matusiak, M.; Kamińska, D. Liquid Moisture Transport in Cotton Woven Fabrics with Different Weft Yarns. *Materials* **2022**, *15*, 6489. [CrossRef]
59. Martí, M.; Gisbert-Paya, J.; Bonet-Aracil, M.Á.; Jovančić, P.; Lis, M.J.; Coderch, L. Increased comfort of polyester fabrics. *Polymers* **2021**, *13*, 3010. [CrossRef]
60. Lee, D.W.; Little, T.J. Difference in hydrophobic and hydrophilic multilayered systems. *Measurement* **2013**, *46*, 920–927. [CrossRef]
61. Zheng, W.; Gao, Y.; Zong, X.; Wang, J. Study on the Properties and Design Applications of Polyester–Cotton Matrix Mycelium Composite Materials. *Biomimetics* **2025**, *10*, 681. [CrossRef] [PubMed]
62. Wang, H.; Peng, J.; Yao, Y.; Liang, Z. A flexible, soft superabsorbent polyester-cotton blended fabric in-situ coated by poly(sodium acrylate-co-acrylic acid). *Mater. Today Commun.* **2024**, *40*, 109358. [CrossRef]
63. Sfameni, S.; Lawnick, T.; Rando, G.; Visco, A.; Textor, T.; Plutino, M.R. Super-Hydrophobicity of Polyester Fabrics Driven by Functional Sustainable Fluorine-Free Silane-Based Coatings. *Gels* **2023**, *9*, 109. [CrossRef]
64. Chen, M.; Deng, X.; Guo, R.; Fu, C.; Zhang, J. Tensile Experiments and Numerical Analysis of Textile-Reinforced Lightweight Engineered Cementitious Composites. *Materials* **2022**, *15*, 5494. [CrossRef]
65. Mu, B.; Meyer, C.; Shimanovich, S. Improving the interface bond between fiber mesh and cementitious matrix. *Cem. Concr. Res.* **2002**, *32*, 783–787. [CrossRef]
66. Ahmad, W.; Khan, M.; Smarzewski, P. Effect of short fiber reinforcements on fracture performance of cement-based materials: A systematic review approach. *Materials* **2021**, *14*, 1745. [CrossRef]
67. Grzesiak, S.; Pahn, M.; Schultz-Cornelius, M.; Harenberg, S.; Hahn, C. Influence of fiber addition on the properties of high-performance concrete. *Materials* **2021**, *14*, 3736. [CrossRef]
68. Raghunath, S.; Hoque, M.; Foster, E.J. On the roles of cellulose nanocrystals in fiber cement: Implications for rheology, hydration kinetics, and mechanical properties. *ACS Sustain. Chem. Eng.* **2023**, *11*, 10727–10736. [CrossRef]

69. Kurpińska, M.; Pawelska-Mazur, M.; Gu, Y.; Kurpiński, F. The impact of natural fibers' characteristics on mechanical properties of the cement composites. *Sci. Rep.* **2022**, *12*, 20565. [CrossRef]
70. Wijesinghe, K.A.P.; Lanarolle, G.; Gunasekara, C.; Hidallana-Gamage, H.D.; Law, D.W.; Wang, L.; Gamage, N.; Gunathilaka, H. Thermal insulation and acoustic absorption performance of textile fibre-reinforced cement mortars. *J. Build. Eng.* **2025**, *111*, 113128. [CrossRef]
71. Tuncel, Y.; Pekmezci, B. Sustainable fiber reinforced cementitious panels containing PCM: Mechanical and thermal performance. *Rev. ALCONPAT* **2020**, *10*, 180–190. [CrossRef]
72. Li, Y.; Yin, S.; Feng, L. Test and analysis of the flexural performance of sandwich insulation wall panels with textile-reinforced engineered cementitious composites in wythes after hot rain cycles. *J. Ind. Text.* **2024**, *54*, 15280837241235396. [CrossRef]
73. Gedif, B.; Atalie, D. Recycling of 100% cotton fabric waste to produce unsaturated polyester-based composite for false ceiling board application. *Int. J. Polym. Sci.* **2022**, *2022*, 2710000. [CrossRef]
74. Gorzelańczyk, T.; Schabowicz, K.; Szymków, M. Tests of fiber cement materials containing recycled cellulose fibers. *Materials* **2020**, *13*, 2758. [CrossRef]
75. Sulochani, R.M.N.; Jayasinghe, R.A.; Priyadarshana, G.; Nilmini, A.H.L.R.; Ashokcline, M.; Dharmaratne, P.D. Waste-based composites using post-industrial textile waste and packaging waste from the textile manufacturing industry for non-structural applications. *Sustain. Chem. Environ.* **2024**, *8*, 100163. [CrossRef]
76. Ailenei, E.C.; Ionesi, S.D.; Dulgheriu, I.; Loghin, M.C.; Isopescu, D.N.; Maxineasa, S.G.; Baciu, I.R. New waste-based composite material for construction applications. *Materials* **2021**, *14*, 6079. [CrossRef]
77. Read, R.E.H. Standard fire tests for building materials and structures. *R. Soc. Health J.* **1981**, *101*, 190–195.
78. Abrams, M.S.; D'Souza, M.V.; Higginson, P.; Metes, W.S.; Quintiere, J.G.; Parker, W.J.; Robins, R.F.; White, J.A., Jr. Review of ASTM test for surface burning characteristics of building materials (E 84)(an ASTM white paper). *J. Test. Eval.* **1985**, *13*, 89–114.